Cutoff solitons and bistability of the discrete inductance-capacitance electrical line: Theory and experiments

K. Tse Ve Koon,[1] J. Leon,[2] P. Marquié,[3] and P. Tchofo-Dinda[1]
[1]*Institut Carnot de Bourgogne, UMR 5209 CNRS, Université de Bourgogne, 9 Avenue A. Savary, Boîte Postal 47 870, 21078 Dijon, France*
[2]*Laboratoire de Physique Théorique et Astroparticules CNRS-UMR5207, Université Montpellier 2, 34095 Montpellier, France*
[3]*Laboratoire LEII, UMR CNRS No. 5158, Université de Bourgogne, Boîte Postal 47870, 21078 Dijon, France*
(Received 8 February 2007; revised manuscript received 27 April 2007; published 8 June 2007)

A discrete nonlinear system driven at one end by a periodic excitation of frequency above the upper band edge (the discreteness induced cutoff) is shown to be a means to (1) generate propagating breather excitations in a long chain and (2) reveal the bistable property of a short chain. After detailed numerical verifications, the bistability prediction is demonstrated experimentally on an electrical transmission line made of 18 inductance-capacitance (*LC*) cells. The numerical simulations of the *LC*-line model allow us also to verify the breather generation prediction with a striking accuracy.

DOI: 10.1103/PhysRevE.75.066604 PACS number(s): 05.45.Yv, 42.65.Tg

I. INTRODUCTION

The response of a nonlinear system to external driving is an extremely rich problem with many interesting fields of application, such as self-induced transparency in a two-level medium [1], propagation of light pulses in waveguides [2], stimulated Raman scattering in H_2 gas [3], transparency of Bragg media in the gap [4], to mention a few. The variety of predicted and observed phenomena comes from the various choices of external excitations and the different natures of intrinsic or extrinsic nonlinearities.

A fundamental class of interesting phenomena is the periodic driven boundary, which consists of exciting a medium at one end with a periodic forcing. Such is the case, for instance, of a chain of short superconducting tunnel junctions coupled through superconducting wires, the so-called Josephson junction parallel array [5], where local excitation (breathers) can be created and propagate down the chain by exciting the first cell only. The periodic driven boundary can also model a scattering problem such as, for instance, in Bragg media (dielectric media with periodic index variation) where the coupled mode approach maps the scattering problem to a boundary value problem [6].

Energy transmission in a nonlinear medium by a periodic driven boundary whose period falls inside a forbidden band gap occurs by means of generation of local structures (solitons) and has been shown to be a universal phenomenon called nonlinear supratransmission [7,14]. It has then been demonstrated to successfully apply to the Josephson junction parallel array [8] and to the Bragg gap soliton generation [9].

One result of the theory of nonlinear supratransmission is a simple and explicit expression for the threshold intensity above which transmission occurs. This knowledge allows one to tune the driving such as to work right below transmission, and thus design a device (detector or switch) that will respond to any weak superimposed signal, either by propagating solitons (or breathers) in the long-line case, or by bifurcating to an excited new state in the short-line case.

All these studies have been performed for systems with band-pass-type dispersion laws, when the external driving frequency was chosen inside the lower forbidden gap, the generated local excitations being thus called gap solitons. A quite natural question then arises whether or not such a phenomenon would still occur in discrete systems above the cutoff. Indeed it is an intrinsic property of a discrete system to possess a cutoff frequency in the dispersion curve (at dimensionless wave number $k=\pi$), above which no propagation of a linear signal can occur. As a matter of fact it has been demonstrated that a Fermi-Pasta-Ulam chain driven above the upper band edge does possess a threshold of nonlinear supratransmission [10].

In view of experimental realization of nonlinear supratransmission and bistability above the cutoff, we study here a particularly interesting device made of a chain of inductance-capacitance cells (*LC*) submitted to a periodic voltage applied to the first cell. The nonlinearity is obtained by using nonlinear capacitor and the system is known to possess interesting properties as modulational instability and soliton propagation [11]. The *LC* chain has a low-pass filter type of dispersion relation (no band gap) and its discrete nature induces an upper edge of the dispersion relation, the cutoff, above which no propagation is allowed for linear waves.

We first demonstrate that a *long line* submitted to periodic forcing slightly above the cutoff, does present a threshold amplitude (frequency dependent) above which solitons are emitted and propagate along the line. A multiscale asymptotic analysis of the model equations allows us to derive the analytic expression of the threshold which is then compared to simulations. The analysis is performed by seeking the evolution equation for the envelope of a wave precisely at the cutoff frequency where the group velocity vanishes, a property that maps the boundary value problem for the line to a well posed boundary value problem for the limit model.

The existence of such a threshold of energy transmission indicates that the system might present a bistable behavior, which could then be experimentally realized on a short line. Indeed we predict analytically the bistability by studying the short line case where the other end of the chain is open. We

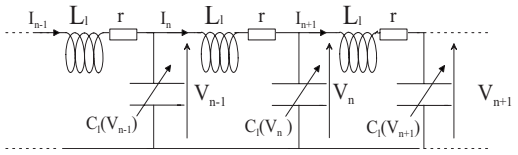

FIG. 1. Standard discrete nonlinear low-pass electrical line.

derive explicit stationary solutions of the limit model and check their validity on numerical solution of the *LC*-line system. The predictions are then experimentally realized with a chain of 18 cells where bistability is evidenced. We have thus obtained the first experimental realization of nonlinear bistability of a discrete system driven at a frequency above the cutoff.

II. THE ELECTRICAL *LC* LINE

The standard nonlinear discrete *LC* line is a structure made of elementary cells which consist of an inductance L, a nonlinear capacitor $C(V)$, and a resistance r, as represented in Fig. 1. The resistance r accounts for the dissipation induced by the inductance L in each elementary cell. The nonlinear element is a voltage dependent capacitor, the BB112 reversed-biased diode. Following Ref. [11] the capacitance-voltage relationship is Taylor expanded to second order and reads (see also Ref. [12])

$$C(\bar{V}+V_n) = C \times [1 - 2\alpha V_n + 3\beta V_n^2], \tag{1}$$

where $\bar{V}$ is the dc bias voltage. We shall operate around $\bar{V}=2$ V, with $|V_n| \leqslant 2$ V, and

$$C = 320 \text{ pF}, \quad L = 220\mu \text{ H},$$

$$\alpha = 0.21 \text{ V}^{-1}, \quad \beta = 0.0197 \text{ V}^{-2}. \tag{2}$$

Applying Kirchoff's laws to this system leads to the following set of propagation equations:

$$\left\{\frac{d^2}{dt^2} + \frac{r}{L}\frac{d}{dt}\right\}(V_n - \alpha V_n^2 + \beta V_n^3) = \frac{1}{LC}(V_{n+1} + V_{n-1} - 2V_n), \tag{3}$$

for $n=1,2,\ldots N$. The corresponding (linear, undamped) dispersion law of the elementary solution $\exp[i(kn-\omega t)]$ is given by

$$\omega = \omega_c \sin(k/2), \quad \omega_c = \frac{2}{\sqrt{LC}}, \tag{4}$$

where ω_c is the cutoff (angular) frequency.

In the case of negligible damping ($r=0$), we consider the modulation (slowly varying in time and space) of a wave which propagates at a carrier angular frequency ω and wave vector k. The solution to Eq. (3) is sought as the formal series

$$V_n(t) = \epsilon[\psi(\xi,\tau)e^{i\theta} + \psi^*(\xi,\tau)e^{-i\theta}] + \epsilon^2[\phi(\xi,\tau) + B(\xi,\tau)e^{2i\theta} + B^*(\xi,\tau)e^{-2i\theta}] + \cdots, \tag{5}$$

$$\xi = \epsilon(n - \omega' t), \quad \tau = \epsilon^2 t, \quad \theta = kn - \omega t, \tag{6}$$

where ϵ is a small parameter and ω' is the group velocity. Substituting Eq. (5) into Eq. (3), the amplitude of the first-order harmonic ψ is found to obey the nonlinear Schrödinger (NLS) equation [13]

$$i\frac{\partial\psi}{\partial\tau} + P(\omega)\frac{\partial^2\psi}{\partial\xi^2} + Q(\omega)|\psi|^2\psi = 0, \tag{7}$$

with the coefficients

$$Q(\omega) = \alpha^2\omega\left(\frac{3\beta}{2\alpha^2} + \frac{\omega_c^2}{\omega^2} - 2\right), \tag{8}$$

$$P(\omega) = \frac{1}{2}\frac{\partial^2\omega}{\partial k^2} = -\frac{\omega}{8}. \tag{9}$$

The dispersion coefficient $P(\omega)$ is thus always negative whereas the nonlinear coefficient $Q(\omega)$ can be positive or negative. Consequently, depending on the carrier wave frequency ω, the NLS equation (7) can be either focusing or defocusing.

III. THE BOUNDARY DRIVEN LINE

The case of interest here corresponds to a carrier wave at the cutoff frequency $\omega=\omega_c$ (and thus $k=k_c=\pi$), which will then obey the nonlinear envelope evolution (7) with now $\omega'(k_c)=0$ (vanishing group velocity) and the coefficients

$$Q(\omega_c) = \frac{1}{2}\omega_c(3\beta - 2\alpha^2), \quad P(\omega_c) = -\frac{1}{8}\omega_c. \tag{10}$$

These two coefficients are both negative and lead to the self-focusing NLS model

$$-i\frac{\partial\Psi}{\partial t} + \frac{\omega_c}{8}\frac{\partial^2\Psi}{\partial x^2} + \frac{1}{2}\omega_c(2\alpha^2 - 3\beta)|\Psi|^2\Psi = 0, \tag{11}$$

where we have scaled off the small parameter ϵ by the inverse transformation $\epsilon\psi=\Psi$, $\epsilon x=\xi$, $\epsilon^2 t=\tau$ such as to have everything written in physical dimensions. Note in particular that the integer values of the variable x are simply n, the discrete variable.

The fact that the group velocity vanishes is fundamental for our task as indeed, the boundary driving of the cell $n=0$ maps to a boundary value problem in $x=0$ for the NLS equation. As a matter of fact, we submit one end of the electrical line ($n=0$) to an external constant amplitude periodic driving

$$V_0(t) = V_0\cos(\omega t), \quad \omega > \omega_c, \tag{12}$$

with a frequency slightly above the cutoff frequency. The linear theory predicts an evanescent wave profile $V_n(t) = V_0\cos(\omega t)\exp(-\kappa n)$ with $\omega=\omega_c\cosh(\kappa/2)$.

In the nonlinear case, following [7], the linear evanescent wave is replaced by the static breather tail that has the frequency (synchronization) and the amplitude (adaptation) of the driver. However the *LC* line does not support explicit

known solitonlike solution (even in the continuous limit). We thus apply the nonlinear supratransmission approach to the NLS approximate description (11). From the relation

$$V_n(t) \simeq \Psi(n,t)e^{i(k_c n-\omega_c t)} + \Psi^*(n,t)e^{-i(k_c n-\omega_c t)} \quad (13)$$

the boundary driving (12) maps to the following boundary value problem:

$$\Psi(0,t) = \frac{1}{2}V_0 e^{-i\omega_s t}, \quad \omega_s + \omega_c = \omega. \quad (14)$$

Driving the line above the cutoff ($\omega > \omega_c$) means then $\omega_s > 0$ and therefore the NLS equation (11) is also driven in the forbidden gap.

We note moreover that the assumption of slow variation (in time) leads to the proper definition of the small parameter ϵ as the relative departure from the cutoff frequency, namely, $\omega_s/\omega_c = \epsilon^2$, which by Eq. (5) also measures the precision of the approximate expression (13).

The static breather solution of Eq. (11) that synchronizes and adapts to the driving eventually reads

$$\Psi_s(x,t) = Ae^{-i\omega_s t}\,\mathrm{sech}[\lambda(x-x_0)], \quad (15)$$

$$A^2 = 4\frac{\omega_s}{\omega_c}\frac{1}{2\alpha^2 - 3\beta}, \quad \lambda^2 = 8\frac{\omega_s}{\omega_c}, \quad (16)$$

where the center x_0 is determined by the boundary condition (14), namely, by the equation

$$A\,\mathrm{sech}(\lambda x_0) = \frac{1}{2}V_0, \quad (17)$$

which has a solution if $V_0 \leqslant 2A$. This is the sought threshold, reached at $x_0 = 0$, which may eventually be written

$$V_{\mathrm{th}} = 4\sqrt{\frac{\omega - \omega_c}{\omega_c(2\alpha^2 - 3\beta)}}. \quad (18)$$

Driving the NLS equation by Eq. (14) with $V_0 > V_{\mathrm{th}}$ produces an instability that allows formation of moving solitons, and thus energy transmission in the line. In the following section, we compare the above analytical predictions with numerical simulations.

IV. CUTOFF SOLITON GENERATION

We have carried out numerical simulations of the *LC* line (3) with vanishing resistance r, submitted to the boundary driving (12) to verify that (i) the generation of cutoff solitons does occur, (ii) this generation is effective only if the amplitude of the external driving exceeds the threshold given by Eq. (18).

To this end, we have considered an *LC* line consisting of 2000 cells for a time of integration that avoids free end reflections. The physical values are given in Eq. (2) and the nonlinear capacitor is the BB112 reversed-biased diode with the characteristics (1). The cutoff frequency is $f_c = 1.1997$ MHz. The propagation equations (3) are integrated by means of a fourth-order Runge-Kutta algorithm with a time step $dt = 2\pi/(200\omega_c)$. The external driving is given by

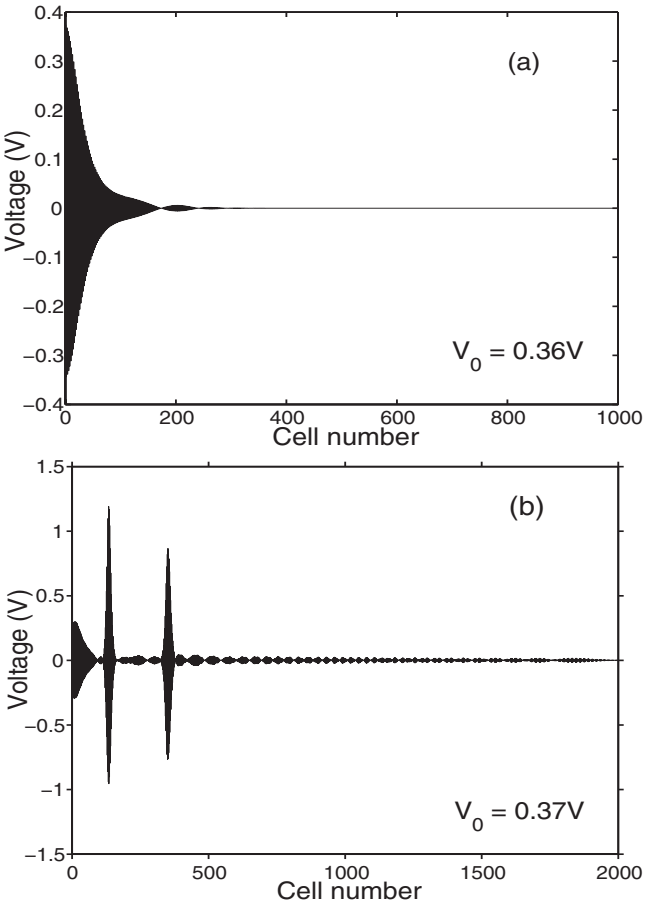

FIG. 2. Final state at time $t = 5$ ms of the electrical line for a driving frequency of 1.2 MHz and amplitudes (a) 0.36 and (b) 0.37 V, both obtained for 2000 cells. The figure (b) shows energy transmission above the threshold 0.37 V as predicted by expression (18).

Eq. (12) after a transient sequence where V_0 grows from a vanishing amplitude to its maximum value so as to avoid initial shock. The total simulation time $t_{\max}$ is set to 5 ms. Figure 2 shows the state of the electrical line at the end of our simulations for two different amplitudes (0.36 and 0.37 V) and for a frequency of 1.2 MHz, for which the prediction (18) gives here the threshold amplitude 0.38 V.

Thus energy propagates for a driving amplitude of 0.37 V whereas 0.36 V produces an evanescent wave. The energy transmission occurs by means of generation of localized structures which propagate through the electrical line, and confirms the existence of an amplitude threshold above which cutoff solitons are generated. To distinguish the generated solitons, we compare on Fig. 3 the results of a numerical simulation of the electric line (3) (the driving signal is spent off as soon as the first soliton is generated) with the analytic expression of the moving soliton solution of Eq. (11), namely, with

$$V_n(t) = \frac{2a\cos[(\delta + k_c)n - (\nu + \omega_c)t]}{\cosh[\mu(t - t_0) - \gamma(n - n_0)]}. \quad (19)$$

This is a solution as soon as the parameters obey

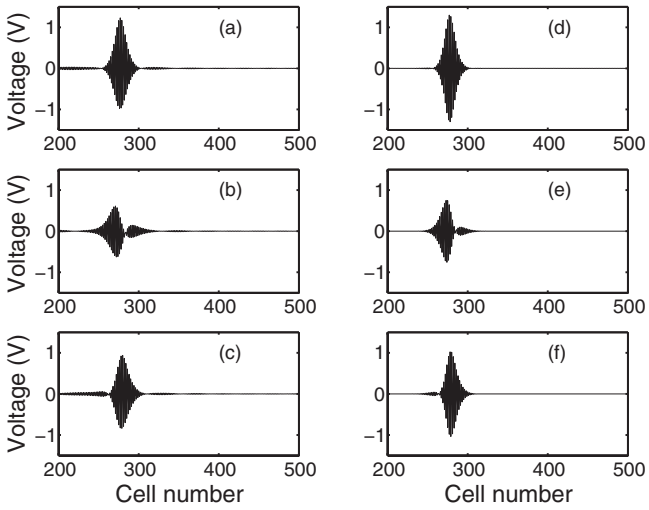

FIG. 3. Comparison between a numerical simulation of the electric line (a)–(c) with the solitonlike solution (19) with parameters given in Eq. (21) (d)–(f).

$$\nu = \frac{\omega_c}{8}(\gamma^2 - \delta^2), \quad \mu = -\frac{\omega_c}{4}\delta\gamma, \quad a^2 = \frac{\gamma^2}{4\alpha^2 - 6\beta}, \quad (20)$$

which are determined by fitting the soliton velocity μ/γ and the phase ν by synchronization to the simulations. The the example displayed on Fig. 3 has been obtained for

$$\mu = 18986\ \mathrm{s}^{-1}, \ \nu = 20939\ \mathrm{s}^{-1}, \quad (21)$$

and hence $a=0.67$ V, $\delta=0.062$, and $\gamma=0.16$. Initial time t_0 and position n_0 are then simply chosen for convenience.

We have carried out systematic simulations to determine the threshold amplitudes at different frequencies in order to compare with the analytical prediction (18). Figure 4 demonstrates excellent agreement between numerical simulations and analytical predictions, although the prediction is made with the slowly varying envelope approximation.

An efficient diagnostic of the bifurcation from evanescent regime to energy transmission by soliton generation is obtained by computing the normalized energy flux received at site i, defined as

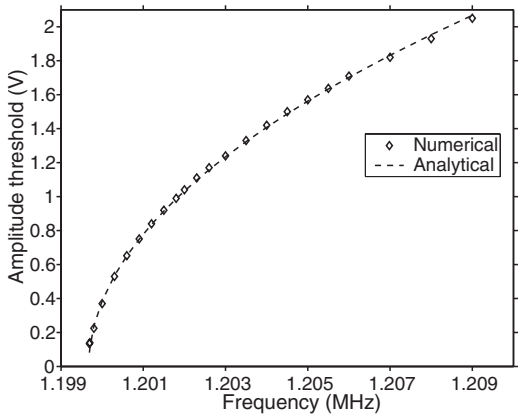

FIG. 4. Comparison between numerical (diamonds) and analytical (dashed line) determination of the threshold amplitudes above which cutoff solitons are generated.

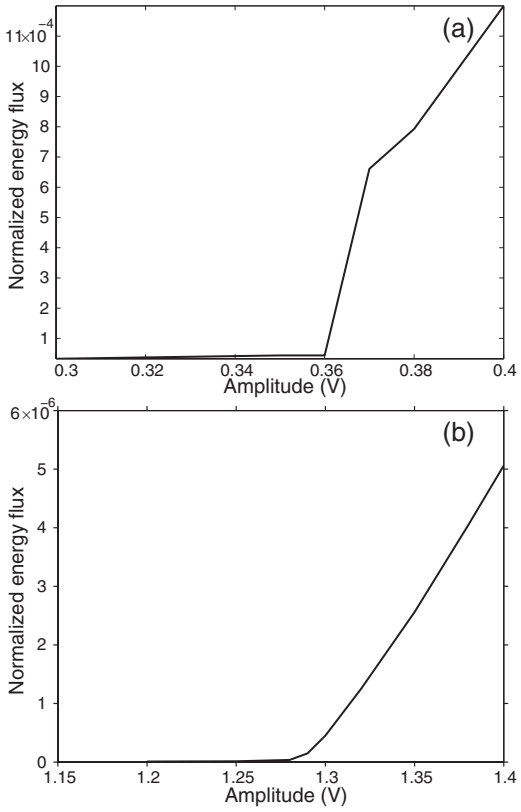

FIG. 5. Normalized energy flux (22) computed numerically on system (3) (with $N=2000$) at cell $i=90$ for a frequency of 1.2 MHz and (a) $r=0$, (b) $r=5\ \Omega$.

$$E_{\mathrm{flux}} = \int_0^{t_{\max}} \left(\frac{V_i(t)}{V_0}\right)^2 dt. \quad (22)$$

The site i is chosen such that, in the absence of propagation, the amplitude of the signal be nearly vanishing. Figure 5 shows the results at $i=90$ for a driving frequency of 1.2 MHz. There is an abrupt increase about $V_0=0.37$ V as expected from the theoretical threshold prediction 0.38 V given by Eq. (18).

Dissipation effects are mainly due to the internal resistance of the inductances, as represented in Fig. 1. Numerical simulations have revealed that the presence of dissipation causes the threshold amplitudes to increase significantly and the energy transmission be more progressive as displayed in Fig. 5(b). For instance, with the values $r=1$, 5, and 10 Ω we have obtained respectively (at frequency 1.2 MHz), the thresholds 0.48, 1.29, and 1.92 V (instead of 0.38 V). As the model (3) holds for amplitudes less than 2 V, we cannot consider higher values of the resistance. However, although dissipation largely limits the propagation of solitons in a long line, a stationary solution may settle in a short line due to the free end reflection. Then, a steady driving excitation may well sustain those waves even with strong dissipation. Therefore we consider hereafter the short-line case defined by a

length which is less than a typical breather extension of about 70 cells in our system.

V. BISTABLE SHORT *LC* LINE

Let us consider the *LC* line of N cells submitted to the boundary conditions

$$V_0(t) = V_0 \cos(\omega t), \quad V_{N+1}(t) = -V_N(t), \tag{23}$$

corresponding to an open end last cell. Indeed, a carrier wave at the cutoff frequency can be written $(-1)^n \cos \omega_c t$ and successive cells work in opposition. The envelope of a carrier wave at cutoff frequency obeys the NLS equation (11) with now, from Eq. (13), the following boundary conditions:

$$\Psi(0,t) = \frac{1}{2} V_0 e^{-i\omega_s t}, \quad \frac{\partial \Psi}{\partial x}(N,t) = 0, \tag{24}$$

where $\omega_s + \omega_c = \omega$.

We work out the explicit stationary solutions of the NLS equation (11) submitted to the above boundary conditions. The fundamental solutions, written in terms of Jacobi elliptic functions, will allow us to prove the existence of bistability, namely the existence of multiple values $V_N(t)$, that we call the output voltage, corresponding to a single input value $V_0(t)$ in a prescribed range. We shall then demonstrate by numerical simulation that the *LC*-line model (3) excited as indicated by Eq. (23), does lock to those analytical solutions. The resulting prediction of bistability will be experimentally realized in the next section with a line of $N=18$ cells which is about one quarter of the typical breather solution extension. Note that bistability here is a nonlinear *collective* process as each cell of the line is not a bistable oscillator.

Let us seek a stationary solution of Eq. (11) that synchronizes to the driver frequency ω_s in the form

$$\Psi(x,t) = \phi(y) e^{-i\omega_s t}, \quad y = 2x\sqrt{2\alpha^2 - 3\beta}, \tag{25}$$

with a scaling of space such that $\phi(y)$ obeys

$$\frac{\partial^2 \phi}{\partial y^2} + \phi^3 = \gamma \phi, \quad \gamma = \frac{\omega_s}{\omega_c} \frac{2}{2\alpha^2 - 3\beta}. \tag{26}$$

The solutions in terms of Jacobi elliptic functions whose derivative vanish at the line end D defined by

$$D = 2N\sqrt{2\alpha^2 - 3\beta}, \tag{27}$$

can be written [15]

$$\phi^{(1)}(y) = A_1 \mathrm{cn}[\kappa_1 (y - D), \mu_1], \tag{28}$$

$$\phi^{(2)}(y) = A_2 \mathrm{dn}[\kappa_2 (y - D), \mu_2], \tag{29}$$

$$\phi^{(3)}(y) = \frac{A_3}{\mathrm{dn}[\kappa_3 (y - D), \mu_3]}, \tag{30}$$

with the following parameter values

$$\kappa_1^2 = \frac{\gamma}{2\mu_1^2 - 1}, \quad A_1^2 = 2\kappa_1^2 \mu_1^2, \tag{31}$$

$$\kappa_2^2 = \frac{\gamma}{2 - \mu_2^2}, \quad A_2^2 = 2\kappa_2^2, \tag{32}$$

$$\kappa_3^2 = \frac{\gamma}{2 - \mu_3^2}, \quad A_3^2 = 2\kappa_3^2 (1 - \mu_3^2). \tag{33}$$

As the above solutions guarantee, by construction, the synchronization of $\Psi(x,t)$ to the driver frequency, we are left with the *adaptation* condition of the amplitudes ϕ^j to the driver amplitude in $x=0$, namely,

$$\phi^{(j)}(0) = \frac{1}{2} V_0, \quad j = 1,2,3. \tag{34}$$

The three related output voltages amplitudes V_j, defined as the maximum value of $V_N^{(j)}(t)$, are then given from the three constants A_j's by

$$A_j = \phi^{(j)}(D) = \frac{1}{2} V_j, \quad j = 1,2,3. \tag{35}$$

These are completely, and uniquely, determined from V_0 as described hereafter.

Writing explicitly the three relations (34) with convenient use of the parameters definitions, we get

$$V_0^2 = \frac{8\gamma\mu_1^2}{2\mu_1^2 - 1} \mathrm{cn}^2 \left[\frac{D\sqrt{\gamma}}{\sqrt{2\mu_1^2 - 1}}, \mu_1 \right], \tag{36}$$

$$V_0^2 = \frac{8\gamma}{2 - \mu_2^2} \mathrm{dn}^2 \left[\frac{D\sqrt{\gamma}}{\sqrt{2 - \mu_2^2}}, \mu_2 \right], \tag{37}$$

$$V_0^2 = 8\gamma \frac{1 - \mu_3^2}{2 - \mu_3^2} \mathrm{dn}^{-2} \left[\frac{D\sqrt{\gamma}}{\sqrt{2 - \mu_3^2}}, \mu_3 \right], \tag{38}$$

while the relations (35) give us

$$V_1^2 = \frac{8\gamma\mu_1^2}{2\mu_1^2 - 1}, \tag{39}$$

$$V_2^2 = \frac{8\gamma}{2 - \mu_2^2}, \tag{40}$$

$$V_3^2 = 8\gamma \frac{1 - \mu_3^2}{2 - \mu_3^2}. \tag{41}$$

As the constants γ and D are given from the line characteristics and from the driving frequency, the remaining parameters μ_j can be eliminated from the above two sets of relations. This yields the three sought relations between the input voltage amplitude V_0 and the three output voltage amplitudes V_j.

Actually the relations (39)–(41) allow us to express explicitly the μ_j's in terms of V_j. As these parameters are the moduli of the Jacobi elliptic functions, they must thus obey $0 < \mu_j^2 < 1$. Consequently the outputs V_j belong also to a given range and we eventually obtain

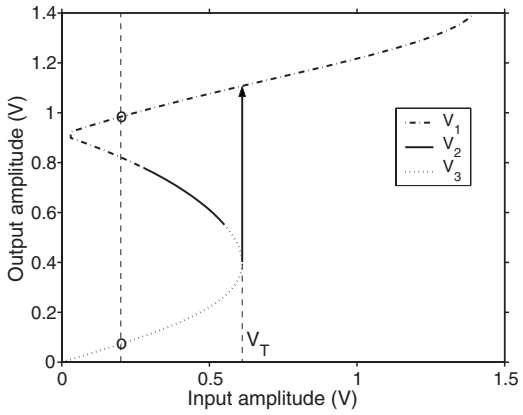

FIG. 6. Output amplitude values expressed in terms of the input amplitude V_0 varying from 0 to 1.4 V for a frequency of 1.201 MHz. The dotted line stands for V_3 expressed in terms of V_0 by Eqs. (41) and (44). The full line is $V_2(V_0)$ given by Eqs. (40) and (43). The dot-dashed line represents $V_1(V_0)$ in Eqs. (39) and (42). The two circles at input amplitude 0.2 V show the values used to draw Fig. 7 representing the related solutions.

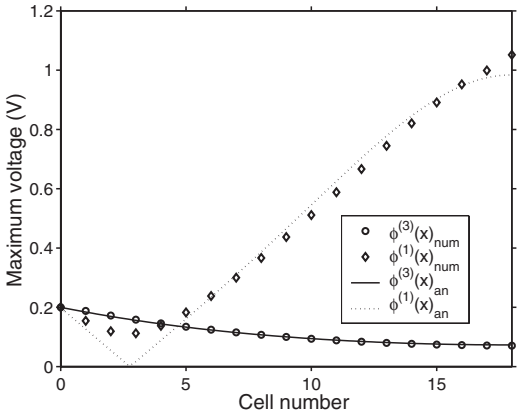

FIG. 7. The profiles of stable solutions at given input driving amplitude V_0=0.2 V. The solution with output V_3 corresponds to expression (30) while the profiles with output V_1 corresponds to expression (28). The horizontal axis is the variable $x=n$. The analytical expressions are compared with numerical simulations (points) as described in the text.

$$\mu_1^2 = \frac{V_1^2}{2V_1^2 - 8\gamma} \in [0,1] \Rightarrow V_1 \in [\sqrt{8\gamma}, \infty], \tag{42}$$

$$\mu_2^2 = \frac{2V_2^2 - 8\gamma}{V_2^2} \in [0,1] \Rightarrow V_2 \in [\sqrt{4\gamma}, \sqrt{8\gamma}], \tag{43}$$

$$\mu_3^2 = \frac{8\gamma - 2V_3^2}{8\gamma - V_3^2} \in [0,1] \Rightarrow V_3 \in [0, \sqrt{4\gamma}]. \tag{44}$$

Reporting the above expressions in Eqs. (36)–(38) give the expression of V_0 in terms of the three V_j's in their respective intervals. It is then just a matter of plotting the obtained functions to get the bistability diagram, as can be seen in Fig. 6, obtained for the values in Eq. (2), for $N=18$ and a driving frequency 1.201 MHz. In the parameter region under consideration

$$\gamma = 0.0759 \text{ V}^2, \quad D = 6.14 \text{ cell V}^{-1}. \tag{45}$$

Figure 6 shows two possible values of the output voltage for the same input voltage amplitude of 0.2 V. The branch with negative derivative corresponds to an unstable solution while the other two branches are stable, as shown by the numerical simulations that follow. The vertical line followed by the arrow shows the threshold of bifurcation whose value is 0.61 V. The vertical dashed line shows the input tension V_0=0.2 V for which the solutions corresponding to two different output tensions (the circles) are plotted in Fig. 7. The solution before bifurcation at the threshold is $\phi^{(3)}(x)_{\text{an}}$ (analogous of the linear evanescent wave) with output V_3, then $\phi^{(1)}(x)_{\text{an}}$ with output V_1.

The threshold of bifurcation, obtained by canceling the derivative of the expression of V_0 in terms of V_3, is found to be equal to 0.61 V, which is below the supratransmission threshold of 0.78 V given by Eq. (18), a formula that holds strictly for $L \to \infty$. Let us also mention that the solution is actually multistable. Figure 6 displays the first threshold, but increasing the vertical axis to large output values would show multiple oscillations of the output V_1.

Before proceeding with an experimental realization of that bistability prediction, it is necessary to check it on numerical simulations of the model (3) of a real *LC* line, in particular with inclusion of dissipation due to the nonvanishing resistance of the inductance *L*. We have thus considered the discrete *LC* line used in Sec. II with now a total length of 18 cells. An extra care is taken so as to avoid initial shock by using a longer transient sequence and integration time (10 ms). As a result, Fig. 8 shows striking agreement between the thresholds obtained analytically with our numerical simulations.

As the energy required to realize bifurcation remains in the system, a stationary stable state will be reached with help of dissipation. We have carried out two different simulations (at ν=1.201 MHz and r=0.5 Ω); first the input voltage is increased steadily to 0.2 V, second it is increased to 0.63 V (the threshold at this frequency and for a null dissipation is equal to 0.61 V) and decreased to the same final value of

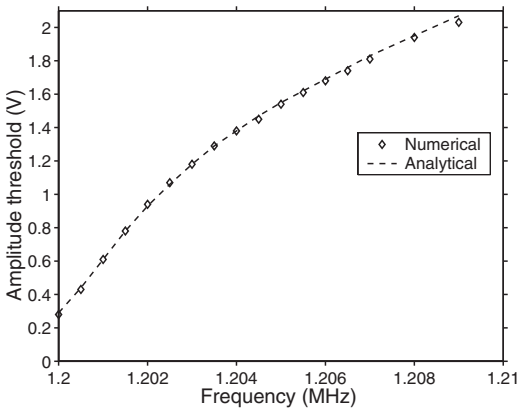

FIG. 8. Comparison between the bifurcation thresholds found numerically (diamonds) and analytically (dashed line) for an eighteen cell line without dissipation.

0.2 V. Figure 7 compares the moduli of the analytical profiles $\phi_{\mathrm{an}}^{(1)}$ and $\phi_{\mathrm{an}}^{(3)}$ with the maximum voltage obtained numerically on the electrical line $\phi_{\mathrm{num}}^{(1)}$ and $\phi_{\mathrm{num}}^{(3)}$. We conclude that agreement between numerical simulations and theory is fully demonstrated.

VI. EXPERIMENTAL RESULTS

In order to compare the numerical results with experimental measures, we first have to consider large resistance values. Indeed, according to our experimental measures, the actual resistance of the inductances for frequencies around 1.2 MHz is of the order of 40 Ω. We have thus carried out numerical simulations so as to determine the thresholds for a frequency of 1.201 MHz. As expected, the thresholds increase with increasing resistance, e.g., 1.5 V for 10 Ω, 3.4 V for 20 Ω, and 4.3 V for 40 Ω.

Now the point is that for large voltage values, the Taylor expansion of the varicap diode (1) is not accurate enough. We have thus used a higher-order expansion given by [16] which reads

$$C(\bar{V}+V_n) = C[1 - 2a_1V_n + 3a_2V_n^2 - 4a_3V_n^3 + 5a_4V_n^4 - 6a_5V_n^5]. \tag{46}$$

For a dc bias voltage of about 2 V, we obtain the following values of parameters:

$$C = 320 \text{ pF},$$

$$a_1 = 0.2 \text{ V}^{-1}, \quad a_2 = 0.0257 \text{ V}^{-2}, \quad a_3 = 0.00222 \text{ V}^{-3},$$

$$a_4 = 1.22 \times 10^{-4} \text{ V}^{-4}, \quad a_5 = 3.5 \times 10^{-6} \text{ V}^{-5}. \tag{47}$$

Another important point is the inductances values that have a tolerance of 5%. This has a drastic consequence on the definition of the theoretical threshold values as illustrated, e.g., by using the formula (4) for the definition of the cutoff frequency and Eq. (18) for the supratransmission threshold to obtain for a driving frequency of 1.23 MHz:

$$L \in [210,230]\ \mu\text{H} \Rightarrow \nu_c \in [1.173,1.228] \text{ MHz},$$

$$V_{\text{th}} \in [0.97,5.15] \text{ V}. \tag{48}$$

Thus 5% of variations of the inductance L induces up to 150% of variation of the supratransmission threshold prediction. A similar evaluation can be made with the values of the varicap which influences also the nonlinear factors. Consequently our experiments will focus on a demonstration of bistable properties of a short electrical LC line together with a qualitative comparison between experimental and numerical results.

We may then proceed to experimental measures on an eighteen cell LC line as drawn in Fig. 1. For a driving frequency of 1.2 MHz, Fig. 9 shows (logarithmic scale) the output voltage versus input voltage (measured at the first cell) which is steadily increased from 1 V to a maximum of 7 V (squares) and is then reduced to 2 V (crosses). The output voltage is defined as half the difference between the maxima and minima measured at cell 18 over a time span of 50 μs. Similarly to Fig. 6, there exists an upper threshold between 5.5 and 5.6 V, where the system bifurcates from nonconducting to conducting regimes. These two different regimes are illustrated in Figs. 10(a) and 10(b).

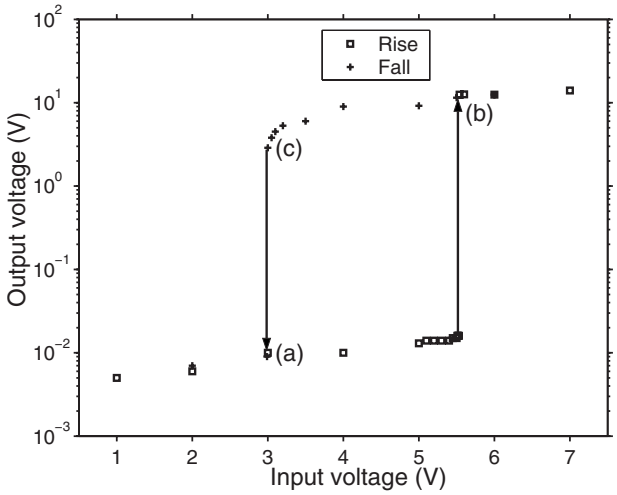

FIG. 9. Experimental hysteresis curve obtained on an 18 cell LC line at $f=1.2$ MHz. The points (a), (b), and (c) indicate the values used to represent the output amplitudes in Fig. 10.

We have carried out similar measures with a frequency varying from 1.2 to 1.3 MHz and obtained that the upper bifurcation threshold steadily varies from 5.5 to 6.7 V. For each frequency, twenty measures were made on two different days. As the measurements of the inductance values were made at room temperature, the experiments with the line never lasted more than an hour to avoid component heating. Temperature may cause significant threshold variations, for instance, at 1.2 MHz, we observed variations in the range 5.5 to 6.2 V. Following this simple rule allowed us to obtain values for the thresholds with a very small dispersion and Fig. 11 displays the results of our measurements (vertical

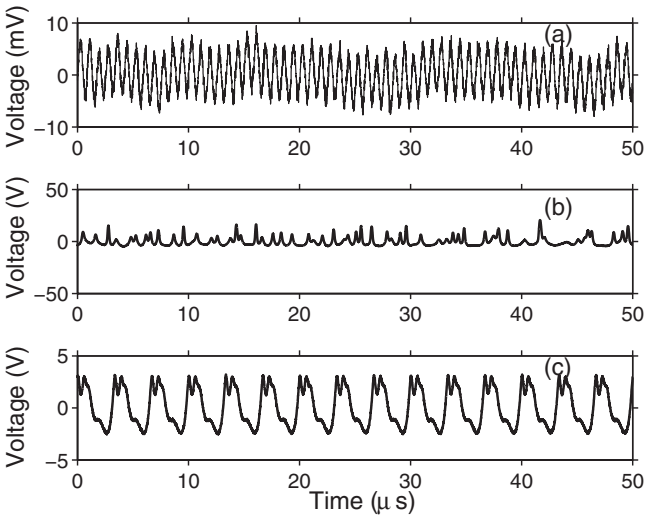

FIG. 10. Signal measured at cell 18 for the three driving amplitudes shown in Fig. 9 at points (a), (b), and (c). Note the different units on vertical axes.

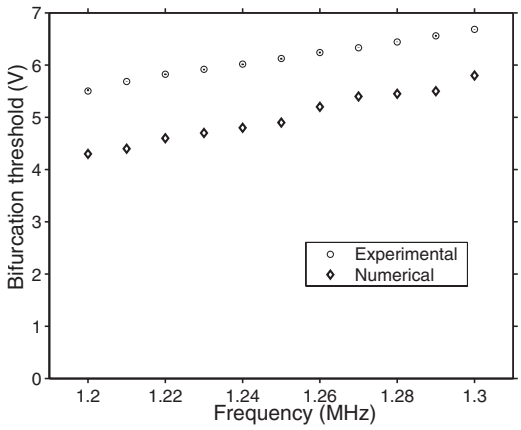

FIG. 11. Bistability threshold measured experimentally (circles) and numerically with a resistance coefficient of 40 Ω (diamond) on an 18 cell line for frequencies varying from 1.2 to 1.3 MHz.

bars show that negligible dispersion). Although the obtained values are different, our numerical simulations have assumed given values of inductance and given Taylor expansion of the capacitance that may not be the actual ones. The interesting result is the correct qualitative agreement seen in Fig. 11 of the threshold variations.

VII. CONCLUSION

We have realized an experimental demonstration of the bistable nature of a discrete nonlinear system driven above the cutoff. Our result is motivated and sustained by a complete theory based on explicit analytical solutions in the conservative case and in the limit of slowly varying envelope approximation. Although dissipation strongly affects the results, we have obtained a reasonable agreement between measures and simulations, while excellent agreement between theory and simulations has been obtained in the weakly dissipative case.

We have established the existence of cutoff solitons and have proposed a very simple way of generating them. Using the NLS limit envelope equation, we have obtained the formula for the threshold amplitude above which soliton generation occurs by nonlinear supratransmission. Our formula agrees extremely well with the numerical simulations, when the driving is performed close to the upper band edge.

In the presence of dissipation, the threshold increases significantly with increasing values of the resistance which affects strongly the solitons generation process. The experimental realization of cutoff soliton generation in the *LC* line requires both a long line and components with low dissipation coefficients (we expect to build a 200-cell electrical line soon).

[1] S. L. McCall and E. L. Hahn, Phys. Rev. **183**, 457 (1969); J. C. Eilbeck, J. D. Gibbon, P. J. Caudrey, and R. K. Bullough, J. Phys. A **6**, 1337 (1973); G. L. Lamb Jr., Phys. Rev. A **8**, 422 (1974); M. J. Ablowitz, D. J. Kaup, and A. C. Newell, J. Math. Phys. **15**, 1852 (1974).

[2] V. E. Zakharov and A. B. Shabat, Sov. Phys. JETP **34**, 62 (1972); A. Hasegawa and F. Tappert, Appl. Phys. Lett. **23**, 142 (1973).

[3] K. Drühl, R. G. Wenzel, and J. L. Carlsten, Phys. Rev. Lett. **51**, 1171 (1983); C. Claude and J. Leon, *ibid.* **74**, 3479 (1995).

[4] D. N. Christodoulides and R. I. Joseph, Opt. Lett. **13**, 794 (1988).

[5] D. Barday and M. Remoissenet, Phys. Rev. B **41**, 10387 (1990).

[6] A. B. Aceves and S. Wabnitz, Phys. Lett. A **141**, 37 (1989); D. N. Christodoulides and R. I. Joseph, Phys. Rev. Lett. **62**, 1746 (1989).

[7] F. Geniet and J. Leon, Phys. Rev. Lett. **89**, 134102 (2002).

[8] D. Chevriaux, R. Khomeriki, and J. Leon, Phys. Rev. B **73**, 214516 (2006).

[9] J. Leon and A. Spire, Phys. Lett. A **327**, 474 (2004).

[10] R. Khomeriki, S. Lepri, and S. Ruffo, Phys. Rev. E **70**, 066626 (2004).

[11] P. Marquié, J. M. Bilbault, and M. Remoissenet, Phys. Rev. E **49**, 828 (1994).

[12] M. Remoissenet, *Waves Called Solitons*, 3rd ed. (Springer, Berlin, 1999).

[13] D. Yemélé, P. Marquié, and J. M. Bilbault, Phys. Rev. E **68**, 016605 (2003).

[14] F. Geniet and J. Leon, J. Phys.: Condens. Matter **15**, 2933 (2003).

[15] R. Khomeriki and J. Leon, Phys. Rev. Lett. **94**, 243902 (2005).

[16] J. Eilbeck, *Numerical studies of solutions on lattices*, in Nonlinear Coherent Structures in Physics and Biology, edited by M. Remoissenet and M. Peyrard, Lecture Notes in Physics 393 (Springer-Verlag, Berlin) p. 143 (1991)